

Quantum teleportation with dissimilar quantum dots over a hybrid quantum network

Alessandro Laneve^{*1}, Giuseppe Ronco¹, Mattia Beccaceci¹, Paolo Barigelli¹, Francesco Salusti², Nicolas Claro-Rodriguez², Giorgio De Pascalis¹, Alessia Suprano¹, Leone Chiaudano¹, Eva Schöll^{†2}, Lukas Hanschke^{‡2}, Tobias M. Krieger³, Quirin Buchinger⁴, Saimon F. Covre da Silva^{3,5}, Julia Neuwirth¹, Sandra Stroj⁶, Sven Höfling⁴, Tobias Huber-Loyola⁴, Mario A. Usuga Castaneda⁷, Gonzalo Carvacho¹, Nicolò Spagnolo¹, Michele B. Rota¹, Francesco Basso Basset¹, Armando Rastelli³, Fabio Sciarrino¹, Klaus Jöns², and Rinaldo Trotta^{§1}

¹Dipartimento di Fisica, Sapienza Università di Roma, Piazzale Aldo Moro 5, I-00185 Roma, Italy

²Institute for Photonic Quantum Systems (PhoQS), Center for Optoelectronics and Photonics Paderborn (CeOPP) and Department of Physics, Paderborn University, Warburger Straße 100, 33098, Paderborn, Germany

³Institute of Semiconductor and Solid State Physics, Johannes Kepler University, Altenbergerstraße 69, Linz 4040, Austria

⁴Technische Physik, University of Würzburg, Am Hubland, D-97074 Würzburg, Germany

⁵Universidade Estadual de Campinas, Instituto de Física Gleb Wataghin, 13083-859 Campinas, Brazil

⁶Forschungszentrum Mikrotechnik, FH Vorarlberg, Hochschulstr. 1, A-6850 Dornbirn, Austria

⁷Single Quantum B.V., Delft, HH 2629, The Netherlands

November 20, 2024

Abstract

Photonic quantum information processing in metropolitan quantum networks lays the foundation for cloud quantum computing [1, 2], secure communication [3, 4], and the realization of a global quantum internet [5, 6]. This paradigm shift requires on-demand and high-rate generation of flying qubits and their quantum state teleportation over long distances [7]. Despite the last decade has witnessed an impressive progress in the performances of deterministic photon sources [8–11], the exploitation of distinct quantum emitters to implement all-photonic quantum teleportation among distant parties has remained elusive. Here, we overcome this challenge by using dissimilar quantum dots whose electronic and optical properties are engineered by light-matter interaction [12], multi-axial strain [13] and magnetic fields [14] so as to make them suitable for the teleportation of polarization qubits. This is demonstrated in a hybrid quantum network harnessing both fiber connections and 270 m free-space optical link connecting two buildings of the University campus in the center of Rome. The protocol exploits GPS-assisted synchronization, ultra-fast single photon detectors as well as stabilization systems that compensate for atmospheric turbulence. The achieved teleportation state fidelity reaches up to $82 \pm 1\%$, above the classical limit by more than 10 standard deviations. Our field demonstration of all-photonic quantum teleportation opens a

^{*}alessandro.laneve@uniroma1.it

[†]current affiliation: Institute of Semiconductor and Solid State Physics, Johannes Kepler University, Altenbergerstraße 69, Linz 4040, Austria

[‡]current affiliation: Walter Schottky Institut, TUM School of Computation, Information and Technology and MCQST, Technical University of Munich, Hans-Piloty Str. 1, 85748 Garching, Germany

[§]rinaldo.trotta@uniroma1.it

new route to implement solid-state based quantum relays and builds the foundation for practical quantum networks.

Large scale quantum networks require the capability of transferring quantum information between distant nodes. Currently, photons represent the best candidate to carry out such a task: they are compatible with pre-existing optical fiber [15] and free-space infrastructure [3], they are extremely resilient to environmental decoherence and they feature a variety of easily manipulable degrees of freedom, for which quantum correlations have been demonstrated [16–19]. More specifically, the flexibility and noise resilience of the polarization degree of freedom makes it the current optimal solution to distribute quantum states and quantum correlations over long distances [7, 20]. However, photon distribution over the globe will inevitably be affected by losses, stressing the need of *quantum relays*, i.e. "devices" that mitigate overall losses by teleporting quantum information between distant nodes of a quantum network [21]. The all-photonic version of quantum relays inherently sets very stringent requirements on the sources of indistinguishable and entangled photon states employed across the network. These include high production rate, wavelength tunability, the need of high photon indistinguishability, and near-unity degree of entanglement, to mention a few. In this perspective, semiconductor quantum dots (QDs) have been under the spotlight for two decades, mainly due to the lack of trade-off between brightness and single photon purity (or degree of entanglement) that is typically plaguing Poissonian sources of light [22]. More specifically, QDs have shown on-demand generation of single and entangled photons with high indistinguishability [23, 24], near-unity degree of entanglement [25], ultra-low multi-photon emission [26] and, most importantly, high brightness [9, 12, 27]. Yet, the use of independent QDs to implement all-photonic quantum teleportation in a quantum relay scenario has evaded demonstration so far. The main reason is that this task demands state-of-the-art single and entangled photon sources to be interfaced via two-photon interference. This, in turn, requires the indistinguishability of photons generated by independent QDs, which inevitably feature dissimilar optical properties. Despite pioneering steps along this direction have been moved [24, 28, 29], the requirements set by all-photonic teleportation protocols are simply too demanding to be met by conventional technologies or cherry-picking approaches. To better explain this hurdle, it is sufficient to consider that the "simple" task of generating single photons with high efficiency and indistinguishability requires the use of sophisticated nanophotonic devices [30–32] that exploit light-matter interaction to boost the flux of QD photons. The level of complexity increases dramatically if QDs are to deliver entangled photons with high efficiency, mainly be-

cause their electronic structure has to be controlled with high accuracy [33] and the generated photon pairs feature dissimilar energies. This usually requires additional manipulation techniques in specifically designed optical cavities [12, 27, 34]. Quantum relays with remote QDs not only require all these provisions to be met, but add an additional twist: the need to interface dissimilar and distant single and entangled photon sources. Considering the efforts required to just gather the necessary ingredients, putting them together may be fairly regarded as a titanic endeavor.

Here, we harness two decades of research in QD quantum photonics to show that this challenge can be overcome. We first fabricate state-of-the-art QDs embedded in Circular Bragg Resonators (CBR) [12] designed to boost the flux of both single and entangled photon pairs. We then use external perturbations, specifically multi-axial strain and magnetic fields, to reshape the electronic structure of dissimilar QDs so as to make them suitable for quantum teleportation. Finally, we take advantage of ultrafast nanowire single photon detectors to mitigate the effects of residual photon distinguishability. These ingredients enable the first demonstration of all-photonic quantum state teleportation with dissimilar QDs in an urban communication scenario, specifically in a hybrid quantum network laid over the Sapienza University campus in Rome.

Our achievement is qualitatively showcased in Fig. 1. Two independent and remote QDs are driven under two-photon resonant excitation (TPE) [35] to generate nearly on-demand photon pairs through the biexciton-exciton radiative cascade [36]. We denote the photon emitted by the exciton recombination as X, and the one after the biexciton recombination as XX (Fig. 1a). The input state $|\phi\rangle$ is prepared in the polarization degree of freedom of the X_1 photons, generated by QD₁ in a first laboratory, acting as Node 1 (see Fig. 1b). This photon is sent to a second laboratory, Node 2, where QD₂ generates the XX_2 - X_2 entangled photon pair. There, the quantum interference between X_1 and X_2 photons enables the teleportation of the $|\phi\rangle$ target state onto the polarization state of XX_2 , which is entangled to X_2 . We first benchmark the teleportation between the two separated nodes 1 and 2 in the Marconi building of the Sapienza Physics Department, realizing the first demonstration of all-photonic quantum teleportation between distinct QDs. Then, the XX_2 photon is sent via a 270 m free-space optical link to a third laboratory in a different building of the campus (named after Fermi), acting as Node 3. The link is equipped with specifically designed synchronization devices, and stabilization systems to compensate for atmospheric turbulence. Overall, we achieve the successful teleportation

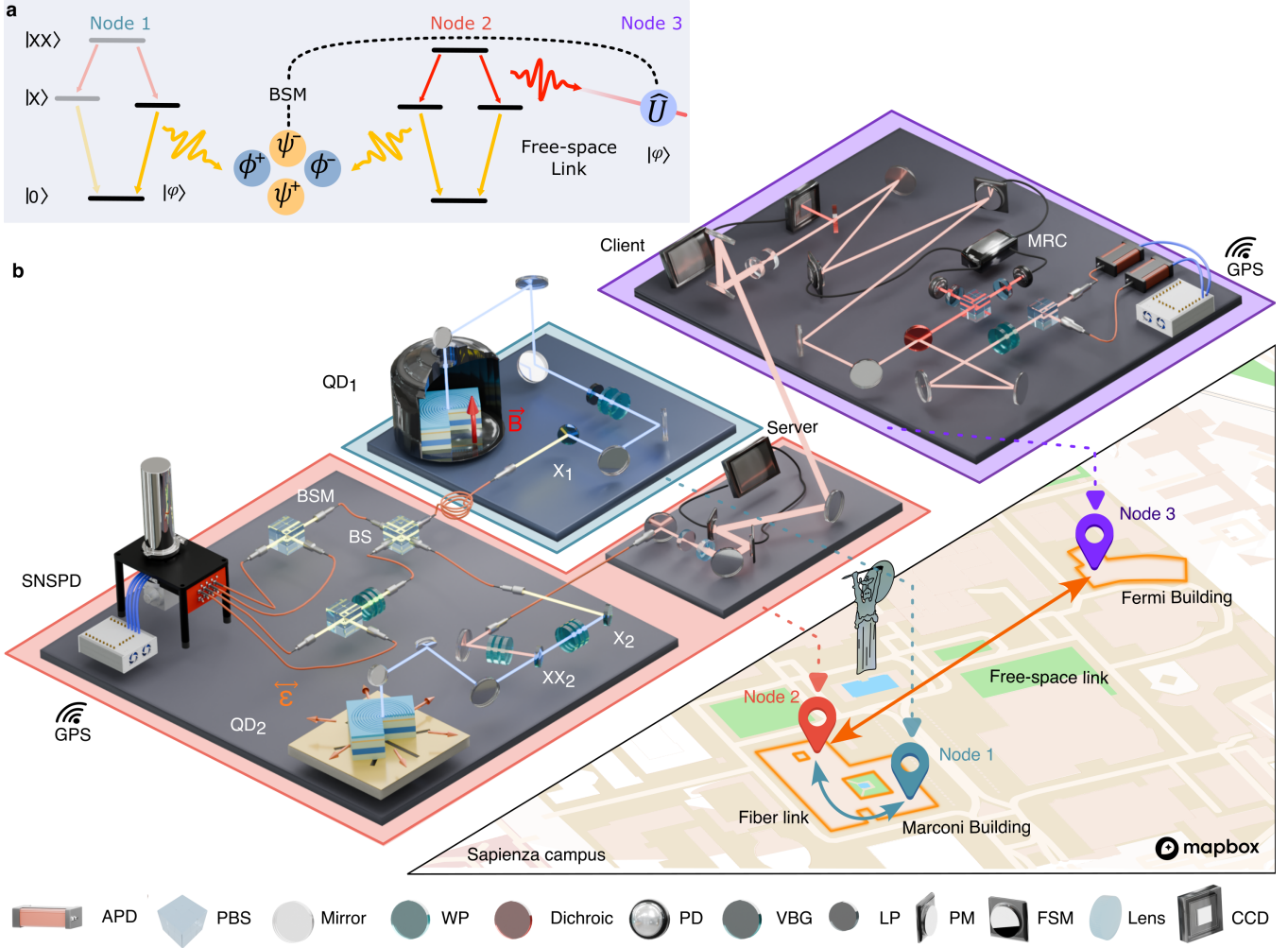


Figure 1: Sketch of the urban quantum teleportation network. *a*, Scheme of the quantum teleportation protocol as implemented with two QDs over a network including a free-space link. *b*, Depiction of the teleportation experimental realization over the Sapienza University campus. In Node 1, highlighted in teal and placed in the Marconi building, the X_1 photon from QD₁ is selected and prepared in a well-defined polarization state. Node 1 is connected with a 15 m optical fibre link to Node 2, highlighted in red, where QD₂ emits a polarization-entangled biexciton-exciton photon pair, XX_2 and X_2 . Spatial displacement between Node 1 and Node 2 is accentuated on the map for clarity. A BSM is performed in Node 2, while XX_2 is sent to Node 3, highlighted in purple and placed in the Fermi building through a 270 m free-space optical link. The strain and the magnetic field harnessed to optimize the X_2 - XX_2 degree of entanglement and the X_1 emission wavelength, are featured in orange and red, respectively. The inset a map of the Sapienza campus, where the Marconi and Fermi buildings are framed in orange. The experimental setup accommodates Volume-Bragg Gratings (VBG), polarizing beam-splitters (PBS), waveplates (WP), piezoelectric mirrors (PM), fast steering mirrors (FSM), and client-server PCs for the optimization of the free-space optical link.

of a polarization qubit using dissimilar QDs in an urban quantum network comprising both fiber and free-space links. The key to the success of the experiments lies in the use of state-of-the-art photonic cavities in combination with innovative quantum-engineering techniques (as sketched in Fig. 1b) to make QD₁ and QD₂ suitable for quantum teleportation, as explained in the next section.

Engineering quantum light sources

For a successful all-photonic quantum teleportation with two remote QDs, three fundamental ingredients are required: (i) a bright source of highly entangled photon pairs; (ii) a bright source of single photons with tunable energy; (iii) the capability to perform a successful Bell state measurement (BSM). We accomplish (i) by

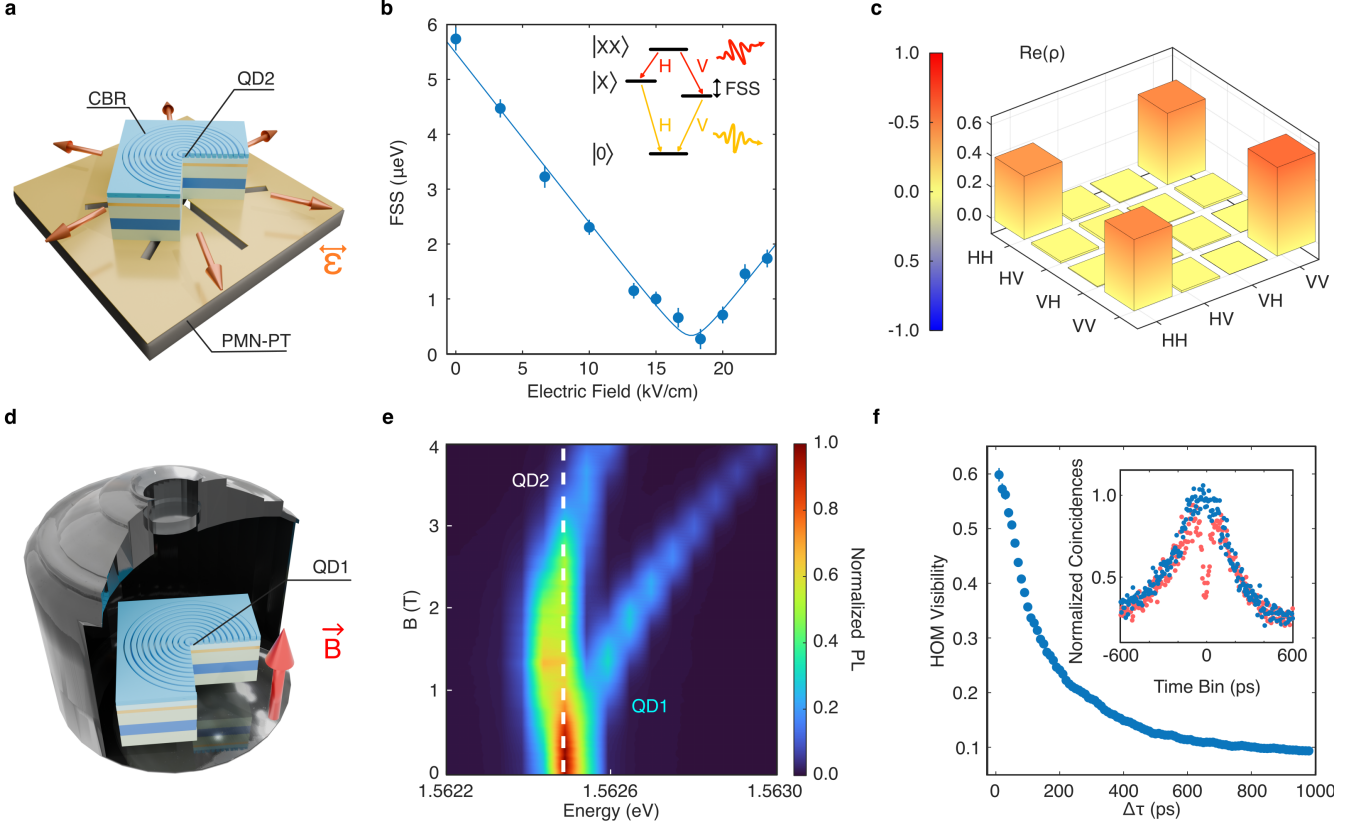


Figure 2: **Quantum resources engineering.** *a*, Schematic representation of the CBR QD integrated onto PMN-PT to enable the application of mechanical stress. *b*, The strain-tuning curve along one axis showing our capability to erase the FSS. The solid line is a fit from the model equations reported in [37]. *c*, Experimental two-photon density matrix (real part) measured for $FSS = 0.3 \pm 0.2 \mu\text{eV}$, yielding a fidelity $F_{|\phi^+\rangle} = 0.94 \pm 0.01$ and a concurrence $C = 0.89 \pm 0.01$. *d* Schematic representation of QD₁ inserted in a magneto-cryostat. *e*, Diamagnetic shift and Zeeman splitting of the emission spectrum of QD₁: thanks to a fine tuning of the B intensity, we achieve spectral overlap between the two X photons applying a magnetic field of $B = 0.9 \text{ T}$. *f*, HOM visibility between photons from remote QDs as a function of the coincidence time window $\Delta\tau$: post-selection on the HOM events allows us to reach a maximum HOM visibility of $V_{HOM} = 0.598 \pm 0.025$ for a 20 ps time window. Inset: time distribution of coincidences in the HOM experiment for co-polarized photon pairs (red) and cross-polarized photon pairs (blue).

using state-of-the-art epitaxial GaAs quantum dots fabricated by the droplet etching method [38]. They can act as bright and reliable sources of single and highly polarization-entangled photon pairs, especially when embedded in suitable photonic structures [12]. In our case, we employ GaAs QDs coupled to circular Bragg resonators (CBRs), also known as bullseye cavities, in turn integrated onto micromachined piezoelectric actuators made of $[\text{Pb}(\text{Mg}_{\frac{1}{3}}\text{Nb}_{\frac{2}{3}})\text{O}_3]_{0.72} - [\text{PbTiO}_3]_{0.28}$ (PMN-PT) [39], as depicted in Fig. 2a. The CBR cavity engineers light-matter interaction to boost the flux of both X and XX photons generated during the radiative cascade. Single-photon (photon-pair) extraction efficiencies as high as 85% (65%) have been demonstrated with this type of cavity [12]. The micro-machined PMN-PT actuators are

instead used to control the QD electronic structure via the application of independent stress fields applied along different crystal directions. These are needed to cancel out the energy splitting between the two X states - the fine structure splitting (FSS) - that is usually induced by asymmetries in the QD confining potential (see Fig. 2b). Erasing this "which-path" information in the radiative cascade is fundamental to obtain near-unity degree of entanglement without temporal post-selection [13, 33, 39]. In our experiment we employ PMN-PT in combination with CBR cavities: by varying the voltages applied to the piezoelectric actuators, we reach a minimum value of $FSS = 0.3 \pm 0.2 \mu\text{eV}$ for QD₂, as reported in Fig. 2b. By performing quantum state tomography on the generated photon pairs we estimate a fidelity of $F = 0.94 \pm 0.01$ to

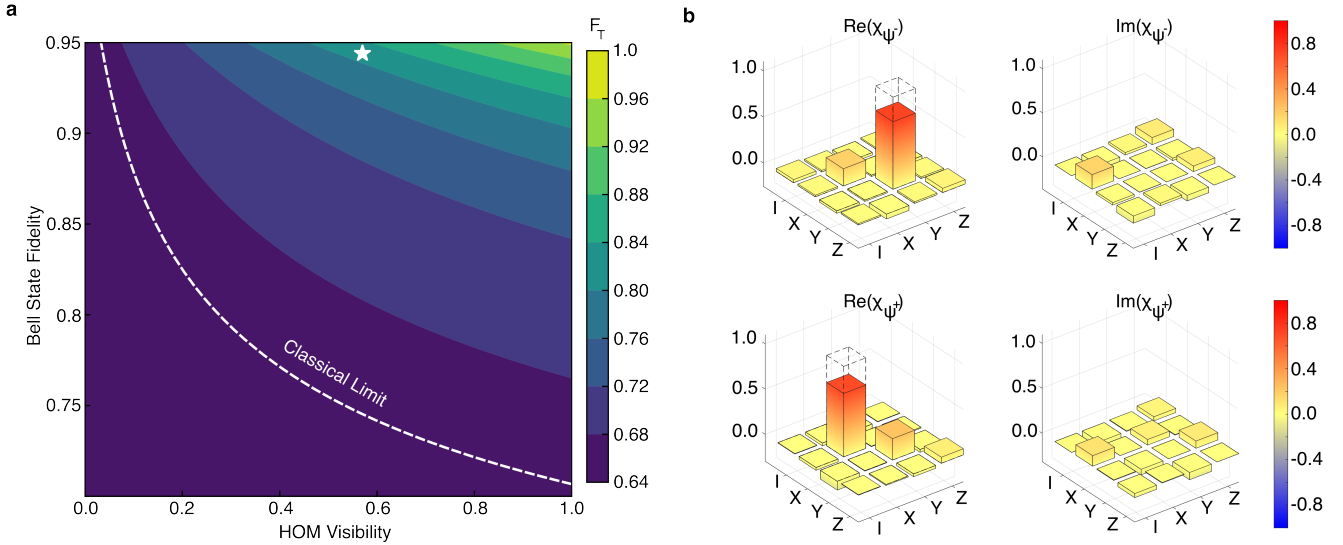


Figure 3: Quantum state teleportation. **a**, Theoretical teleportation fidelity as a function of the quantum resources available for the protocol, computed for the case of a 50% BSM. The white curve highlights the maximum achievable fidelity with classical resources, i.e. for a protocol only relying on classical correlations. The white star points out the expected teleportation fidelity as estimated with our theoretical model. In particular, our Bell state fidelity is 0.94 ± 0.01 and the HOM visibility for 30 ps coincidence window is $V_{\text{HOM}} = 0.57 \pm 0.02$, that yield an average teleportation fidelity $F_T = 0.827 \pm 0.006$. **b**, Experimental process matrices $\chi_{\psi^{\pm}}$ for the teleportation protocol, as defined in [43], reported both for the projection on $|\psi^-\rangle$ (top) and $|\psi^+\rangle$ (bottom), and in comparison with the corresponding ideal process matrix (dashed). The matrices are represented in terms of the quantum operations I (the identity), $X = \sigma_X$, $Y = -i\sigma_Y$ and $Z = \sigma_Z$, where $\{\sigma_{X/Y/Z}\}$ are the Pauli matrices.

the $|\phi^+\rangle$ Bell state without resorting to any time-filtering procedure (see Fig. 2c), close to the best obtained with QDs in optical microcavities [39]. The source of the teleported qubit (ii) is another GaAs QD embedded in a CBR cavity, denoted as QD₁, driven under TPE and generating X_1 and XX_1 photons. The latter are not relevant for the teleportation protocol discussed here and they will not be considered further. The X_1 photon features a wavelength similar to X_2 - but not identical by several radiative linewidths. This is a clear indication that the two independent QDs feature slightly different size, shape or alloy intermixing [40]. In order to achieve spectral indistinguishability between X_1 and X_2 , we employ a magnetic field that shifts the emission by the combination of Zeeman splitting and diamagnetic shift. More specifically, we select one of the Zeeman-split X_1 transitions and use the magnetic field to tune its energy in resonance with the X_2 photon, as reported in in Fig. 2d-e. This step is crucial to achieve (iii). In its most efficient implementation with linear optics, a BSM exploits two photons that interfere on a symmetric beam splitter (BS) coming from two distinct input ports. Then, they undergo a polarization projective measurement at the two output ports, allowing to sample two of the four Bell states, $|\psi^+\rangle$ and $|\psi^-\rangle$. To perform a successful BSM, the impinging photons have to be indis-

tinguishable in all degrees of freedom. While the magnetic field tuning allows us to achieve energetic resonance, X_1 and X_2 feature also different lifetimes and linewidths, a consequence of a slightly different Purcell effect as well as different interaction with the solid-state environment. This can be indirectly observed in the Hong-Ou-Mandel (HOM) interference measurement of X_1 - X_2 photon pairs (realized by performing cross- and co-polarized interference, see the inset of Fig. 2f), exhibiting the typical "volcano shape" [41, 42]. Collecting all the photons coming out from the BS results in a limited HOM visibility, an evidence which can be fully explained by the lifetimes and linewidths of the X_1 and X_2 photons (see the SI). However, the level of indistinguishability can be improved by post-selecting two-photon interference events via ultrafast superconductive nanowire single photon detectors (SNSPDs) and a time-to-digital converter with 19 ps time resolution (FWHM). By narrowing down the considered coincidence detection window $\Delta\tau$, we can achieve HOM visibilities as high as 60% (see Fig. 2f), a value limited by the SNSPDs time resolution. This technique clearly comes at the cost of the number of useful three-fold coincidences exploitable for the teleportation protocol, but not as much as one would intuitively expect. In fact, we point out that the teleportation fidelity that can be

achieved in an experiment depend on both the degree of entanglement and photon-indistinguishability, and overcoming the classical limit is possible even if the available quantum resources are unbalanced, i.e., even with imperfect and dissimilar quantum dots. We have explored this possibility by using a model that computes the maximum theoretically achievable teleportation fidelity as a function of the degree of entanglement in the X_2 - XX_2 photon pair (which is influenced by FSS and quantified by the fidelity of the photon pair state to the $|\phi^+\rangle$ Bell state) and the indistinguishability of the X_1 - X_2 photons (measured by their HOM visibility). The details of the model are reported in the SI while the achieved results are illustrated in Fig. 3a. For the characteristics of our emitters, the predicted teleportation fidelity is $F_T = 0.827 \pm 0.006$, represented by a white star in Fig. 3a. Most importantly, the same figure highlights that the classical limit can be overcome even with a poor HOM visibility (below 20%) in combination with a high level of Bell state fidelity (above 90%). This suggests that successful teleportation with our independent QDs can be achieved by a loose temporal post-selection, at moderate expenses of teleportation rates. This is exactly what motivated our field demonstration of quantum teleportation, as presented in the next section.

Teleportation protocol over a quantum network

The protocol we used builds upon the scheme employed in one of the seminal demonstration of quantum teleportation [44]. We perform the experiment by preparing X_1 photons in the target polarization states $|\phi\rangle$ in laboratory 1 and sending them through a 15 m single-mode fiber to laboratory 2, where they interfere with the X_2 photons through the BSM. At the same time, the XX_2 photons undergo a polarization measurement in laboratory 2, where we collect the three-fold coincidences among their detection and X_1 - X_2 coincidence events in the chosen projection of the BSM. After the X_1 - X_2 interference, the joint polarization state of X_1 - X_2 - XX_2 can be written as [45]:

$$|\Psi\rangle = \frac{1}{2}(|\phi^+\rangle_{X_1, X_2} \hat{I} + |\psi^+\rangle_{X_1, X_2} \hat{\sigma}_X + -i|\psi^-\rangle_{X_1, X_2} \hat{\sigma}_Y + |\phi^-\rangle_{X_1, X_2} \hat{\sigma}_Z) |\phi\rangle_{XX_2}$$

where \hat{I} is the identity operator and $\hat{\sigma}_{X/Y/Z}$ are the Pauli operators.

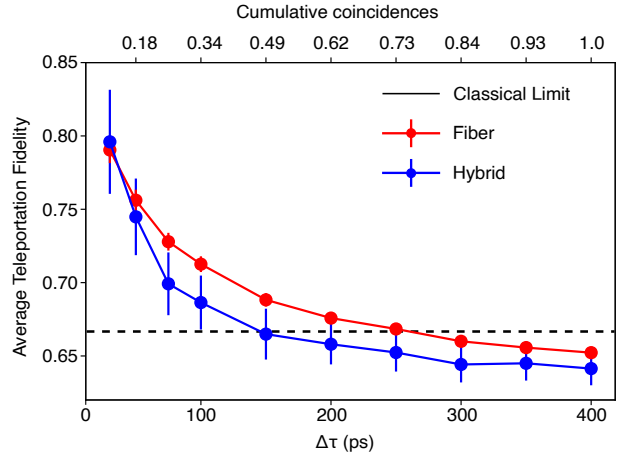


Figure 4: **Temporal post-selection of quantum teleportation events.** Teleportation fidelity averaged over the $|\psi^-\rangle$ and $|\psi^+\rangle$ projections as a function of the BSM coincidence time window $\Delta\tau$. We compare the results obtained for the fiber network case (red points) with the hybrid scenario (blue points), where teleported photons are sent over a 270 m free-space channel. On the top axis, the fraction of retained events over the total (corresponding to a coincidence time window of 400 ps) is reported as a function of $\Delta\tau$.

The BSM projection on one of the two Bell states $|\psi^-\rangle$ and $|\psi^+\rangle$ corresponds to the application of a different operation to the teleported qubit. The whole teleportation protocol from X_1 to XX_2 can be fully characterized by performing a quantum process tomography [43], which yields the *process matrix*. By collecting the three-fold coincidences for different input states, we can reconstruct the teleportation process matrix for different values of BSM coincidence time-window $\Delta\tau$. Those are reported for both projections and for $\Delta\tau = 30$ ps in Fig. 3b. From these matrices, we estimate the overall teleportation fidelity which is found to be $F_T^- = 0.82 \pm 0.01$ for the $|\psi^-\rangle$ projection and $F_T^+ = 0.77 \pm 0.01$ for the $|\psi^+\rangle$ one. Both values are well above the classical limit of $\frac{2}{3}$ [46] by more than 10 standard deviations. Yet, it is worth noting that in the $|\psi^+\rangle$ projection case, we do not reach the theoretical limit of $F_T = 0.827 \pm 0.006$ estimated for our QDs. This is due to unavoidable setup imperfections and other sources of undesired background signal. In particular, we estimate that a slightly imperfect polarization compensation procedure may have decreased the teleportation fidelity for the $|\psi^+\rangle$ projection of around 2%. We provide further discussion of these points in the SI. As mentioned above, our scheme uses temporal post-selection and we investigate how the teleportation fidelity changes as a function of $\Delta\tau$. The red plot in Fig. 4 displays the teleportation results averaged over the $|\psi^-\rangle$ and

$|\psi^+\rangle$ projections applying different coincidence time windows to the BSM up to $\Delta\tau = 30$ ps. It can be clearly seen that the classical limit can be overcome by a relatively moderate temporal post-selection, with a $\Delta\tau$ of about 250 ps. This value allows to retain more than 70% of the total three-fold coincidence events, corresponding to ≈ 30 Hz rate of teleportation events. The best teleportation fidelity is obtained for the $\Delta\tau = 30$ ps window, that allows to retain about 11% of the maximum possible teleportation rate, corresponding to a ≈ 4 Hz teleportation. These results stimulated us to explore the possibility to implement our teleportation scheme in an urban communication scenario, specifically using the Sapienza free-space link [47, 48]: a 270 m free space channel laid over the university campus in the city center of Rome. Rather than being locally analyzed, XX_2 photons are sent through the quantum channel and measured in laboratory 3, in the Fermi building of Sapienza. This operation presents many challenges, including the presence of substantial losses (almost 90% of the signal is lost through the channel), the need to synchronize photon detection, as well as the presence of atmospheric turbulence which makes the coupling of the signal to single mode fibers unstable. The synchronization and instability issues are alleviated by the employment of GPS disciplined oscillators and a stabilization system based on both slow and fast steering mirrors, respectively [47]. The results are shown in Fig. 4, where we report the teleportation fidelities we obtain for a given $\Delta\tau$, in comparison with those achieved in the fiber-only network (see SI for details). Given the losses present in the free-space link, the uncertainty on the fidelity values is considerably larger with respect to the fiber-only network. However, for $\Delta\tau = 30$ ps, we obtain an average teleportation fidelity of $F_T = 0.80 \pm 0.04$, more than 3σ above the classical limit. The slightly lower teleportation fidelities that can be observed in the hybrid network are related to the presence of the free-space channel, which favors the teleportation of some polarization states in comparison with others, due to imperfect polarization compensation procedures. We discuss these points in more detail in the SI.

Discussion and outlook

In this work, we present the first demonstration of all-photonic quantum state teleportation using photons generated by independent and dissimilar quantum emitters, specifically epitaxial QDs. We also successfully scaled up the protocol in an urban quantum network that presents several challenges, including photon losses, atmospheric turbulence, and the need of synchronizing different nodes. We achieve this results by overcoming some of the roadblocks that have long prevented the implementation of

such protocol with quantum emitters. The key to this accomplishment was the use of strain- and magnetic-field-tunable QDs embedded in nanophotonic cavities and the exploitation of state-of-the-art techniques for single photon detection and event analysis. This allowed us to surpass the classical threshold for state teleportation while retaining more than 70% of the total events rate. Moreover, we recorded an average fidelity of up to $79 \pm 1\%$ for about 11% of the total teleportation events. Our achievement now opens an avenue for the development of practical quantum networks and will stimulate additional research endeavors. In fact, several approaches can be put in place to reach near-unity teleportation fidelities at the maximum possible rates. First, the implementation of electric fields to suppress charge noise [49] will allow improving the indistinguishability of photons generated by remote QDs. This possibility has been demonstrated for single photon sources [24], but additional efforts are still needed to improve the brightness of the devices and extend the method to entangled photon sources. Regarding the free-space link, the integration of adaptive optics for compensation of high-order aberrations due to atmospheric turbulence as well as the use of efficient synchronization strategies may allow reducing photon losses to the minimum possible. Although all these tasks will require considerable effort, our demonstration of quantum teleportation in an urban communication scenario highlights that the implementation of a QD-based quantum network for quantum information processing is a likely perspective in the foreseeable future.

References

1. Barz, S. *et al.* Demonstration of blind quantum computing. *Science* **335**, 303–308 (2012).
2. Maring, N. *et al.* A versatile single-photon-based quantum computing platform. *Nature Photonics* **18**, 603–609 (2024).
3. Yin, J. *et al.* Entanglement-based secure quantum cryptography over 1,120 kilometres. *Nature* **582**, 501–505 (2020).
4. Paraiso, T. K. *et al.* A photonic integrated quantum secure communication system. *Nature Photonics* **15**, 850–856 (2021).
5. Kimble, H. J. The quantum internet. *Nature* **453**, 1023–1030 (2008).
6. Wehner, S., Elkouss, D. & Hanson, R. Quantum internet: A vision for the road ahead. *Science* **362**, 9288 (2018).
7. Ren, J.-G. *et al.* Ground-to-satellite quantum teleportation. *Nature* **549**, 70–73 (2017).

8. McKeever, J. *et al.* Deterministic generation of single photons from one atom trapped in a cavity. *Science* **303**, 1992–1994 (2004).
9. Somaschi, N. *et al.* Near-optimal single-photon sources in the solid state. *Nature Photonics* **10**, 340–345 (2016).
10. Ding, X. *et al.* On-demand single photons with high extraction efficiency and near-unity indistinguishability from a resonantly driven quantum dot in a micropillar. *Physical review letters* **116**, 020401 (2016).
11. Tomm, N. *et al.* A bright and fast source of coherent single photons. *Nature Nanotechnology* **16**, 399–403 (2021).
12. Liu, J. *et al.* A solid-state source of strongly entangled photon pairs with high brightness and indistinguishability. *Nature Nanotechnology* **14**, 586–593 (2019).
13. Huber, D. *et al.* Strain-tunable GaAs quantum dot: A nearly dephasing-free source of entangled photon pairs on demand. *Physical Review Letters* **121**, 033902 (2018).
14. Bayer, M., Walck, S., Reinecke, T. & Forchel, A. Exciton binding energies and diamagnetic shifts in semiconductor quantum wires and quantum dots. *Physical Review B* **57**, 6584 (1998).
15. Mao, Y. *et al.* Integrating quantum key distribution with classical communications in backbone fiber network. *Optics express* **26**, 6010–6020 (2018).
16. Kwiat, P. G. Hyper-entangled states. *Journal of Modern Optics* **44**, 2173–2184 (1997).
17. Mair, A., Vaziri, A., Weihs, G. & Zeilinger, A. Entanglement of the orbital angular momentum states of photons. *Nature* **412**, 313–316 (2001).
18. Simon, C. & Poizat, J.-P. Creating single time-bin-entangled photon pairs. *Physical Review Letters* **94**, 030502 (2005).
19. Tanzilli, S. *et al.* A photonic quantum information interface. *Nature* **437**, 116–120 (2005).
20. Yin, J. *et al.* Satellite-based entanglement distribution over 1200 kilometers. *Science* **356**, 1140–1144 (2017).
21. Gisin, N. & Thew, R. Quantum communication. *Nature photonics* **1**, 165–171 (2007).
22. Lodahl, P. Quantum-dot based photonic quantum networks. *Quantum Science and Technology* **3**, 013001 (2017).
23. Schöll, E. *et al.* Resonance fluorescence of GaAs quantum dots with near-unity photon indistinguishability. *Nano Letters* **19**, 2404–2410 (2019).
24. Zhai, L. *et al.* Quantum interference of identical photons from remote GaAs quantum dots. *Nature Nanotechnology* **17**, 829–833 (2022).
25. Huber, D. *et al.* Highly indistinguishable and strongly entangled photons from symmetric GaAs quantum dots. *Nature Communications* **8**, 15506 (2017).
26. Schweickert, L. *et al.* On-demand generation of background-free single photons from a solid-state source. *Applied Physics Letters* **112** (2018).
27. Dousse, A. *et al.* Ultrabright source of entangled photon pairs. *Nature* **466**, 217–220 (2010).
28. Gao, W. *et al.* Quantum teleportation from a propagating photon to a solid-state spin qubit. *Nature Communications* **4**, 2744 (2013).
29. Schimpf, C. *et al.* Quantum dots as potential sources of strongly entangled photons: Perspectives and challenges for applications in quantum networks. *Applied Physics Letters* **118** (2021).
30. Santori, C., Fattal, D., Vuckovic, J., Solomon, G. S. & Yamamoto, Y. Indistinguishable photons from a single-photon device. *Nature* **419**, 594–597 (2002).
31. Ates, S. *et al.* Post-Selected Indistinguishable Photons from the Resonance Fluorescence of a Single Quantum Dot in a Microcavity. *Physical Review Letters* **103**, 167402 (2009).
32. Gazzano, O. *et al.* Bright solid-state sources of indistinguishable single photons. *Nature Communications* **4**, 1425 (2013).
33. Bayer, M. *et al.* Fine structure of neutral and charged excitons in self-assembled In (Ga) As/(Al) GaAs quantum dots. *Physical Review B* **65**, 195315 (2002).
34. Gregersen, N., McCutcheon, D. P., Mork, J., Gerard, J.-M. & Claudon, J. A broadband tapered nanocavity for efficient nonclassical light emission. *Optics Express* **24**, 20904–20924 (2016).
35. Jayakumar, H. *et al.* Deterministic photon pairs and coherent optical control of a single quantum dot. *Physical review letters* **110**, 135505 (2013).
36. Glässl, M. & Michler, P. On-demand generation of indistinguishable polarization-entangled photon pairs. *Nature Photonics* **8**, 224–228 (2014).
37. Trotta, R. *et al.* Universal Recovery of the Energy-Level Degeneracy of Bright Excitons in InGaAs Quantum Dots without a Structure Symmetry. *Physical Review Letters* **109**, 147401 (2012).

38. Gurioli, M., Wang, Z., Rastelli, A., Kuroda, T. & Sanguinetti, S. Droplet epitaxy of semiconductor nanostructures for quantum photonic devices. *Nature Materials* **18**, 799–810 (2019).
39. Rota, M. B. *et al.* A source of entangled photons based on a cavity-enhanced and strain-tuned GaAs quantum dot. *Light* **4**, 13 (2024).
40. Schliwa, A., Winkelkemper, M. & Bimberg, D. Few-particle energies versus geometry and composition of In_xGa_{1-x}As/GaAs self-organized quantum dots. *Physical Review B* **79**, 075443 (2009).
41. Legero, T., Wilk, T., Hennrich, M., Rempe, G. & Kuhn, A. Quantum beat of two single photons. *Physical Review Letters* **93**, 070503 (2004).
42. Schöll, E. *et al.* Crux of using the cascaded emission of a three-level quantum ladder system to generate indistinguishable photons. *Physical Review Letters* **125**, 233605 (2020).
43. Chuang, I. L. & Nielsen, M. A. Prescription for experimental determination of the dynamics of a quantum black box. *Journal of Modern Optics* **44**, 2455–2467 (1997).
44. Bouwmeester, D. *et al.* Experimental quantum teleportation. *Nature* **390**, 575–579 (1997).
45. Rota, M. B., Basset, F. B., Tedeschi, D. & Trotta, R. Entanglement teleportation with photons from quantum dots: toward a solid-state based quantum network. *IEEE J. Sel. Top. Quantum Electron.* **26**, 1–16 (2020).
46. Massar, S. & Popescu, S. Optimal extraction of information from finite quantum ensembles. *Physical Review Letters* **74**, 1259 (1995).
47. Basso Basset, F. *et al.* Quantum key distribution with entangled photons generated on demand by a quantum dot. *Science Advances* **7**, eabe6379 (2021).
48. Basset, F. B. *et al.* Daylight entanglement-based quantum key distribution with a quantum dot source. *Quantum Science and Technology* **8**, 025002 (2023).
49. Kuhlmann, A. V. *et al.* Transform-limited single photons from a single quantum dot. *Nature Communications* **6**, 8204 (2015).

Acknowledgements

This project has received funding from the European Union’s Horizon 2020 research and innovation program

under Grant Agreement no. 899814 (Qurope) and No. 871130 (Ascent+), and from the QuantERA II program that has received funding from the European Union’s Horizon 2020 research and innovation program under Grant Agreement No 101017733 via the project QD-E-QKD and the FFG grant no. 891366. The authors also acknowledge support from MUR (Ministero dell’Università e della Ricerca) through the PNRR MUR project PE0000023-NQSTI, the Linz Institute of Technology (LIT), the LIT Secure and Correct Systems Lab, supported by the State of Upper Austria, the European Union’s Horizon Europe research and innovation program under EPIQUE Project GA No. 101135288, and the European Commission by project QUID (Quantum Italy Deployment) funded in the Digital Europe Programme under the grant agreement No 101091408. This work is supported by the Deutsche Forschungsgemeinschaft (German Research Foundation) through the transregional collaborative research center TRR142/3-2022 (231447078) and the European Research Council starting grant (LiNQs, 101042672).

Author contributions

A. L., G. R., M. B., G. D. and M. B. R. performed the experiment over the fiber network under the supervision of F. B. B. and R. T.. A. L., G. R., M. B., G. D. and M. B. R. performed the experiment over the hybrid network on the Marconi side of the free-space channel under the supervision of F. B. B. and R. T.. P. B. and A. S. participated to the experiment on the Fermi side of the free-space channel under the supervision of G. C., N. S. and F. Sc.. F. Sa., N. C. R. and K. J. contributed to the experimental setup implementation. F. Sa. and P. B. developed the data acquisition code with supervision of F. B. B., A. L., K. J., N. S., G. C. and F. Sc.. A. L., G. R., M. B. and G. D. analyzed the data. F. B. B. developed the model for the expected quantum teleportation performances. L. C. contributed to the setup and characterization of the free-space channel. E. S., L. H., J. N. performed preliminary experiments and studies under the supervision of K. J. and R. T.. S. F. C. d. S. and A. R. designed and grew the QD sample. M. B. R., T. M. K. and Q. B. designed and processed the cavity of the QD with the supervision of R. T., A. R., T. H. L. and S. H.. S. S. processed the micro-machined piezoelectric actuator. M. A. U. C. developed the fast single-photon detectors for the experiments. A. L. and R. T. wrote the paper with contribution from all the authors. R. T. conceived the experiment. A. R., F. Sc., K. J. and R. T. coordinated the project.